Research Article

Space-time CE/SE method for solving repulsive chemotaxis model

Attia Rabbani[1] · **Waqas Ashraf**[1] · **Ubaid Ahmed Nisar**[2]

Received: 9 May 2019 / Accepted: 1 May 2020 / Published online: 28 May 2020

Abstract
This work is concerned with the numerical investigation of nonlinear mathematical systems that describe repulsive chemotaxis phenomena in biology. A space-time conservation element (CE) and solution element (SE) method-based splitting procedure is proposed in one space dimension. In chemotaxis, the orientation of the cells changes. They move to the location which are chemically more favorable or move away from repellents or toxin. Mathematically, these are the systems of nonlinear coupled partial differential equations. The analytical solutions for this set of equations is not possible. A traditional less order accurate solution may fail to describe the underlying phenomena. Therefore, the state of the art numerical procedures is the need for such systems to get physically reliable solution in acceptable computational cost. Unlike tradition numerical procedures, the CE/SE-method has distinct attributes like it treats time and space in a unified fashion. Both conserved quantities and corresponding derivatives are considered to be unknowns due to which inherited numerical diffusion is reduced. Several benchmark numerical test problems are simulated for validation of the scheme. The numerical solutions of case studies are obtained for one space dimension. Moreover, one more central numerical scheme introduced by Nessyahu–Tadmor (NT) is also adapted on staggard grids which is considered to be a black box solver for such models for comparison. It was observed that both schemes perform well for the current mathematical model. However, the CE/SE scheme is more capable of capturing the peaks produced in the solution profile. Further, convergence study is also carried out from both schemes which reveal that the proposed method is fast as compared to NT central scheme.

Keywords Repulsive chemotaxis · Parabolic model · CE/SE method · Solution convergence · NT-central method

1 Introduction

As opposed to diffusion (irregular diffusion), chemotaxis is one-sided cells movement in area which consist of higher beneficial concentration or lower destructive concentration of chemical substances. In general,it introduce attractive (positive) chemotaxis and then finally repulsive (negative) chemotaxis. Few common cases for natural species encountering chemotaxis are incorporate sludge shape amoebae Dictyostelium discoideum [1, 2], flagellated microscopic organisms Escherichia coli [3–5], Myxococcus xanthus [6] and Salmonella Typhimurium [7]. In last 3 decades, chemotaxis research suggests notably excessive ratio of more than 95% among a few works examining taxis.

1.1 Why logarithmic?

The history of the model might be discussed and particularly the importance of the function of logarithmic sensitivity. Article distributed in 1966 in the field of science [8], Adler revealed a critical test result for Escherichia coli. In investigation, Escherichia coli groups seen to move at uniform speed when the microbes set in one end of a narrow tube contained energy source

✉ Attia Rabbani, attia.rabbani@yahoo.com | [1]Department of Applied Mathematics and Statistics, Institute of Space Technology, Islamabad, Pakistan. [2]Department of Applied Mathematics, National University of Technology, Islamabad, Pakistan.

SN Applied Sciences (2020) 2:1133 | https://doi.org/10.1007/s42452-020-2864-3

and oxygen. After four years, in a progression of original works [9–11], Keller and Segel built up a successful numerical model known as Keller–Segel Chemotaxis Model (KSCM). In general form, the Keller–Segel model defined as

$$\frac{\partial u}{\partial t} = \nabla \cdot (D\nabla u - \chi u \nabla \phi(u)), \tag{1}$$

$$\frac{\partial v}{\partial t} = \epsilon \Delta v + g(u, v). \tag{2}$$

where the density of cell is u, v is concentration of chemical, $\epsilon \geq 0$ and $D > 0$ denote coefficients of cell and chemical diffusion, respectively. If $\chi > 0$ then chemotaxis is referred to as attractive (positive) and repulsive (negative) if $\chi < 0$, where $|\chi|$ estimates the chemical signal strength. Here $\phi(v)$ is known as a function of chemotactic potential specifying signal mechanism and function g(u, v) describes the decadence and chemical development.

The regular cases of chemotactic capacity function $\phi(v)$ associated with $\phi(v) = klogv$, $\phi(v) = kv$, or $\phi(v) = kv^m(1 + v^m)$, where $m \in N$ and $k > 0$. The framework with direct law $\phi(v) = kv$ and $g(u, v) = u - v$ are known as the minimum chemotaxis model following [12] and [13]. The logarithmic affect ability $\phi(v) = klogv$ adjusted the Weber-Fechner law to depict cell chemotactic reaction and had unmistakable specific applications [11, 14]. The consistent conditions of Eqs. (1) and (2) with logarithmic sensitivity and $g(u, v) = u - v$ was contemplated [15] and presence of global solutions was as of late examined in [16]. The receptor sensitivity law has been inferred and connected in the various chemotaxis models, e.g. see [17, 18] and references therein.

In this article, we combined model Eqs. (1) and (2) with logarithmic chemotactic potential function and $g(u, v) = uv - \mu v$. The subsequent model [19, 21, 22] is described as follows

$$\frac{\partial u}{\partial t} = \nabla \cdot (D\nabla u - \chi u \nabla \ln(v)), \tag{3}$$

$$\frac{\partial v}{\partial t} = \epsilon \Delta v + uv - \mu v. \tag{4}$$

The constant $\mu > 0$ representing the reduction rate of chemicals. At the point when the chemical diffusion is ignored (i.e. $\epsilon = 0$), Eqs. (3) and (4) were look like to the one proposed in [20, 21] for irregular motion of particles portraying molecule cooperation with a non-diffusive model. In light of unique selection of initial date and by the asymptotic investigation, an itemized subjective and numerical investigation was given in [20], where explicit solutions about aggregation, explode and crumple were developed in one space dimension. The worldwide presence of the solutions examined in [22].

If $\chi < 0$, with a Hopf–Cole type transformation

$$\mathbf{q} = \frac{\nabla v}{v} = \nabla \ln(v), \tag{5}$$

furthermore, scalings $\bar{x} = \sqrt{-\chi}\mathbf{x}, \bar{q} = \mathbf{q}/\sqrt{-\chi}$ and $\tilde{t} = -\chi t/D$ can be transformed within a system of conservation laws [24–26] as takes after

$$p_t - \nabla \cdot (pq) = \Delta p, \tag{6}$$

$$\mathbf{q}_t - \nabla(\epsilon q^2 + p) = \epsilon \Delta \mathbf{q}. \tag{7}$$

Where $q = u$. The existence and nonlinear stability of wave solutions of Eqs. (6) and (7) in one-dimensional space R were built up in [23–25] first for $\epsilon = 0$ and afterward in [26] for $\epsilon > 0$, where the wave quality is permitted to be discretionary extensive. At the point when $\epsilon = 0$, global presence of the classical solutions of underlying IBVP Eqs. (6) and (7) in one dimension space were set up in [27] and the Cauchy problem of Eqs. (6) and (7) was considered in [28]. The Cauchy problem of Eqs. (6) and (7) with $\epsilon = 0$ in multi-dimensional spaces was explored in [29]. As of late the substantial time presence of classical solutions of underlying IBVP of model Eqs. (6) and (7) with $\epsilon = 0$ in one dimensional space with extensive initial data and in multi-dimensional spaces for small-scale initial data were set up [30]. In this paper, our aim is to investigate intial-boundary value problem [31]with $\epsilon > 0$, in one dimension, as follows

$$p_t - (pq)_x = p_{xx}, \tag{8}$$

$$q_t - (\epsilon q^2 + p)_x = \epsilon q_{xx}. \tag{9}$$

For the setup of large-time behavior of classical solutions for $\epsilon > 0$, in one-dimensional space and the diffusion limits of solutions as $\epsilon \to 0$, we build up assessments in [30]. We take note of that the diffusion limit of traveling wave solutions was beforehand gotten in [32]. To show our principle outcomes, we present a few symbols.

It is, for most of the part, trusted that diffusion has a regularization effect. So we assume that the results for $\epsilon = 0$ can be expanded to the case $\epsilon > 0$, but the presence of the convection-like term $(q^2)_x$ creates additional difficulty in the asymptotic analysis. In standard, such a form of nonlinearity does not cause any inconvenience for small-scale solution results, while the situation is changed for solution results with large amplitude. It is clearly that, when ϵ is enormous, the nonlinear convection can never again be influenced by the linear diffusion, and the resulting time-dependent energy estimation gives no informative data for the solution with long-time behavior. This is the principal

reason that we require ϵ to be small. Inside this system of the parameter, by receiving the concept in [30], we can set up the uniform-in-time and ϵ that result in the long-time straight-line behavior of large amplitude solutions. Therefore the uniform convergence rate of the solutions of Eqs. (8) and (9) towards those of the non-diffusive issues. The mathematical framework of repulsive chemotaxis is represented as a system of differential equations. These differential equations are highly nonlinear mathematical models comprised of time-dependent coupled partial differential equations (PDEs). Traveling pulses of chemotaxis are investigated in [33]. A commonly required property of chemotaxis models is that their solutions rapidly grows in the vicinity of concentration points. The solutions of these models are very complicated as it may blow up in finite time or may lead to a very singular and spiky behavior. This blow-up is termed as cell concentration phenomena that occur in real biological systems. In any case, it is very challenging for a numerical scheme to capture such solutions. Similar models have been investigated numerically in [34, 35], where high order methods were developed using the cartesian coordinate system. Wang [36] also investigated mathematics of traveling waves in chemotaxis through numerical techniques about the relevant chemotaxis model which corresponds to the model (1)–(2) by the Cole-Hopf transformation. High performance parabolic chemotaxis model in one space dimension examined in [37]. In this system unique global smooth solution attains convergence when time approaches to infinity. While, it has been shown that solutions of chemotaxis model converge towards their boundary data at an exponential rate when time becomes infinite [38]. Wang et al [39] study the stability of solutions of hyperbolic system in which diffusion limit (viscous limit) of solutions like chemical diffusion ϵ approaches to zero with convergence advice on solutions to the non-diffusible (non-viscous) problem. Even for the transformed system (1)–(2), there are many interesting qualitative results with numerical simulations [40, 41]. However, it was seen that to capture high resolution of density peaks, very fine mesh has to be taken which has a negative impact on the efficiency of the methods. Therefore, it is highly desirable to have robust numerical methods for the implementation and further mathematical and biological analysis of these systems. A considerable attention is given to this area in the past two decades [42, 43]. However, there is still a need for the more efficient and reliable numerical procedures having an acceptable order of accuracy (usually second-order) for such nonlinear models. Therefore, the main emphasis of this work is to suggest a relatively new numerical procedure called space-time CE/SE algorithm for these model equations. Further, the numerical accuracy of the scheme and computational cost is also discussed to favor this numerical method.

The proposed CE/SE scheme is a second-order high resolution and have capability for capturing shocks and steep changes which was introduced by Chang and his team [44]. This scheme is different and relatively new numerical procedure as compared to other traditional numerical methods, like Discontinuous Finite Element (DFE), Finite Volume (FV) and Finite Difference (FD) Methods. The proposed methods have distinct features such as introduction of conservation elements (CE's) and Solution Elements (SE's), treatment of time and space variables in a unified manner, treatment of derivatives of the dependent variable as unknown and shock handling technique without the use of Riemann solvers. Moreover, this numerical framework has successfully shown its generic feasibility and effectiveness with models having complicated solution structure. These models include the unsteady flows [44, 45], radiation hydrodynamics [46], hyperbolic heat conduction scenarios [47], vortex dynamics [48], shallow flow systems [49], magnetohydrodynamics [50] and electrical engineering [51]. The current model equations are also solved using high resolution and non-oscillatory Nessyahu and Tadmore NT central scheme [52] for the comparison and validation of the recommended numerical scheme. This NT schemes are considered as black-box solver for such model equations. These schemes belong to the class of predictor-corrector (PC)-type numerical procedure and hence implemented in two different steps. The average values of the conserved quantities are predicted first using a non-oscillating piecewise linear interpolating polynomial. Afterward, the average values on staggered grids along with predicted averages are used to update the values at the next time level. These schemes are second-order accurate by the virtue of MUSCL type initial reconstruction process. On one hand, these schemes are similar to upwind schemes as they use similar limiters to avoid oscillation. On the other hand, they are different and simple than upwind schemes as they do not require complicated Riemann solvers to be recuperated for the solution.

The CE/SE scheme is designed on different and unique fundamentals as compared to other traditional methods for solving such model equations. Like, upwind finite volume [53, 54] and Discontinuous Galerkin methods [55]. Since solution elements in the proposed numerical framework are staggering both in space and time, therefore, evaluation of the fluxes at the interfaces of cell is easier and consistent. The essential characteristics of flux evaluations include [45]: (a) The calculation of flux requires no interpolation or extrapolation since it lies inside the solution element. Moreover, this solution element is determined by a rule that has no dependence on local numeric profile $i - e$ the complexities of upwind techniques are entirely bypassed in the current method. (b) as mentioned earlier,

flux evaluation is straight forward as it requires integration of first-order Taylor expansion only. The much-complicated strategies like characteristic speed based strategies are not appreciated. For up to second-order accuracy, the CE/SE-scheme is a better choice as compared to Discontinuous Galerkin methods (DGM). However, DGM is suitable for high order accuracy requirements. For that, interpolating polynomials which are similar to WENO limiters are required [56, 57].

The main aim of this article is to extend the CE/SE scheme [58] for the nonlinear mathematical models introduced for repulsive chemotaxis in one space dimension. The current numerical procedure has already been extended successfully to several other engineering models whose solutions are complicated as well. The numerical diffusion is controlled well in these frameworks due to its limiter and treatment of derivatives as independent unknowns. Different benchmark test problems are simulated to verify the comprehensive application and ability of the current recommended numerical algorithm. Moreover, accuracy study is also carried out through both schemes (CE/SE scheme and Nesyyahu Tadmore central scheme) which reveals that the proposed method is more accurate and fast as compared to NT central scheme.

The remaining part of this article is organized as follows. In Sect. 2 , the formulation of proposed numerical schemes in one-dimension is presented. Some numerical test problems for different case studies are discussed in Sect. 3. Finally, conclusions are drawn in Sect. 4.

2 Numerical scheme

In this article, we will discuss and reformulate the compact form of our given model and will also derive the proposed numerical technique.

2.1 Compact form of model and CE/SE method in one space dimension

The compact form of the repulsive chemotaxis model and the numerical scheme will be described in the present part. Repulsive chemotaxis model Eqs. (6) and (7) can be presented in one space dimension as given below.

$$V_t - F(V)_x - E(V)_{xx} = S(V). \tag{10}$$

The vector form of given equation is expressed as:

$$V = \begin{bmatrix} p \\ q \end{bmatrix}, \qquad F(V) = \begin{bmatrix} -pq \\ -(\epsilon q^2 + p) \end{bmatrix}, \qquad S(U) = \begin{bmatrix} 0 \\ 0 \end{bmatrix},$$

where, V is the unknown function, $F(V)$ denotes the function of flux and function of source is represented by $S(V)$.

$$(p,q)(x,o) = (p,q)(x), \quad x \in [0,1], \quad . \tag{11}$$

$$p_x(0,t) = p_x(1,t) = 0, \quad q_x(0,t) = q_x(1,t) = 0, \tag{12}$$

CE/SE [44] suggested numerical scheme applied on model equations. The main idea and methodology is totally different with respect to other existing methods like as FVM and FEM. The unified treatment of time and space is the salient feature of CE/SE method. As studied, in the literature [44, 59, 60], the different types of fluxes are produced. One dimensional CE/SE scheme is illustrated in [44]. The Eq. (13) is defined as

$$\frac{\partial V_k}{\partial t} + \frac{\partial F_k(V)}{\partial x} = S_k(V), \quad k = 1, 2. \tag{13}$$

Let the two coordinates which represents (E_2) space are x and t which are denoted as x_1 and x_2 respectively. Assuming a smooth solution profile, we apply Gauss-divergence theorem on Eq. (13). This gives the following integral form

$$\oint_{S(V)} d_k . ds = S_k. \tag{14}$$

Here V is an arbitrary domain in E_2-space with boundary S(V). The $dS = d\sigma n$ where $d\sigma$ represents area and n is the unit normal outward vector of the surface (element). By applying the CE scheme on Eq. (18) shows discontinuities but on the other hand when SE scheme applied on Eq. (13) it shows different behavior of the curve as compared the result of the CE scheme.

The mesh points j and n in two dimensional space is represented by the set Ω. Where $n, j = 0, \pm 0.5, \pm 1.5, \ldots$. The solution element is linked with each point $(j, n) \in \Omega$, where $j = n \pm 0.5, n \pm 1.0, n \pm 1.5, \ldots,$. and represented as shaded region in Fig. 1a, which is the line segment about the vertical and horizontal axis and their very close neighboring region (exact length of neighboring region is of no importance).

The values of V_k, F_k and d_k are approximated as $V^*{}_k, F^*{}_k$ and $d^*{}_k$. Where

$$V^*{}_k(t, x; j, n) = (V_k)_j^n + (V_{kt})_j^n (t - t^n) + (V_{kx})_j^n (x - x_j). \tag{15}$$

$(V_k)_j^n, (V_{kt})_j^n$ and $(V_{kx})_j^n$ are constant values in $SE(j, n)$. After applying chain rule we have

$$(F_{kx})_j^n = (F_{k,l})_j^n (V_{kx})_j^n, \tag{16}$$

$$(F_{kt})_j^n = (F_{k,l})_j^n (V_{kt})_j^n, \tag{17}$$

where

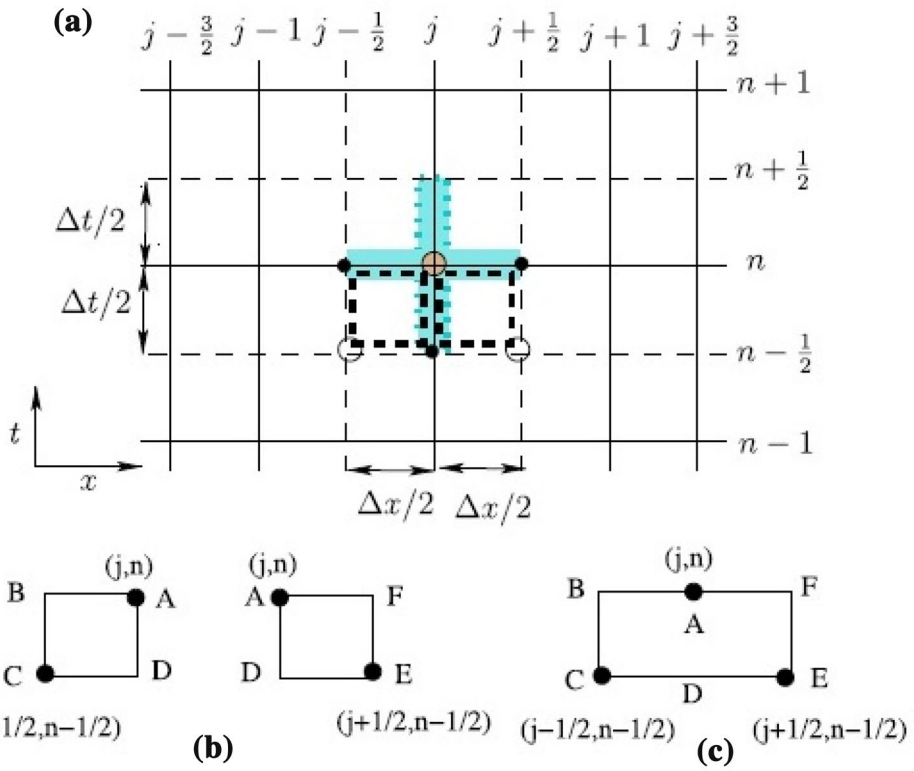

Fig. 1 **a** Space-time staggered grid near $SE(j, n)$. **b** $CE\_(j, n)$ and $CE_+(j, n)$, respectively. **c** $CE(j, n)$

$$F_{k,l} = \frac{\partial F_k}{\partial V_l}, \quad k, l = 1, 2. \tag{18}$$

In Eqs. (16)–(18), F_k and $F_{k,l}$ are the splitting values of $(F_{k,l})_j^n$, respectively. The $A_{k,l}$ for $k, l = 1, 2$ is jacobian matrix where k, l are column and row indices.

From Eqs. (16) and (17), the terms $\frac{\partial F_k}{\partial x}$ and $\frac{\partial F_k}{\partial t}$ are the partial derivatives with respect to position and time respectively. The numerical values of $\frac{\partial F_k}{\partial x}$ and $\frac{\partial F_k}{\partial t}$ are defined as, $(F_{kx})_j^n$ and $(F_{kt})_j^n$ respectively.

$$F^*{}_k(t, x; n, j) = (F_k)_j^n + (F_{kt})_j^n(t - t^n) + (F_{kx})_j^n(x - x_j). \tag{19}$$

$$S^*{}_k(t, x; n, j) = (S_k)_j^n + (S_{kt})_j^n(t - t^n) + (S_{kx})_j^n(x - x_j). \tag{20}$$

As density is defined as, $d_k = (F_k, V_k)^T$,then

$$d_k^*(t, x; n, j) = (F_k^*(t, x; j, n), V_k^*(t, x; j, n))^T. \tag{21}$$

Furthermore, F_k^* and V_k^* satisfy the above Eq. (10), i.e.,

$$\frac{\partial V_k^*(t, x; j, n)}{\partial t} + \frac{\partial F_k^*(t, x; j, n)}{\partial x} = S_k^*(t, x; j, n). \tag{22}$$

From Eqs. (15) and (20), Eq. (22) takes the following form

$$(V_{kt})_n^j = (F_{kx})_j^n + (S_k)_j^n. \tag{23}$$

As $(V_k)_j^n$ and $(V_{kt})_j^n$ are functional values of $(V_{kx})_j^n$. In in similar way in Eq. (23 $(V_k)_j^n$ and $(V_{kx})_j^n$ are the functional values of $(V_{kt})_j^n$. Then applying the same procedure on $((V_k)_j^n$ and $(V_{kt})_j^n$ are also the functional values of $(V_{kt})_j^n$, $(F_k)_j^n$, $((F_{kx})_j^n$ and $(F_{kt})_j^n$ respectively. Let $E - 2$ space contains non overlap regions (see Fig. 1a)refereed to be conservation elements(CEs). Similarly, as presented in Fig. 1b conservation elements $CE\_(j, n)$ and $CE_+(j, n)$ are linked with interior mesh points. These CE'S are referred as basic conservation elements (BCE's). On the other hand, Fig. 1c represents the union of these BCE's $CE_+(j, n)$ and $CE\_(j, n)$, which is called compounded conservation element (CCE).

As observed line segment $CE_+(j, n)$, formed a boundary along $SE(j, n)$, which is denoted by AB and AD. whereas line segments CB and CD belongs to $SE(j - 1/2, n - 1/2)$. In the same fashion boundary of $CE_+(j, n)$ is contained in $SE(j, n)$ or $SE(j + 1/2, n - 1/2)$. Then, by enforcing the two conservation condition at every interior mesh point, we get

$$\oint_{S(CE_{\pm}(j,n))} d_k^* \cdot ds = S_k, \quad k = 1, 2. \tag{24}$$

From the above equation, it is revealed that if the boundary does not intersect by applying basic conservation element then total flux must be zero. The total flux vanishes

at any space-time region. Thus at this stage a union of both positive and negative conservation elements considered and is represented through $CE(j,\ n)$

$$\oint_{S(CE_{\pm}(j,n))} d_k^*.ds = S_k, \quad (j,n) \in \Omega. \tag{25}$$

From Eqs. (24),(15),(19) and (20), one can easily get the following time marching numerical algorithm ,

$$\begin{aligned}(V_k)_n^j = \frac{1}{2}\Big((V_k)_{n-\frac{1}{2}}^{j-\frac{1}{2}} + (V_k)_{k+\frac{1}{2}}^{j-\frac{1}{2}} \\ + (S_k)_{n-\frac{1}{2}}^{j-\frac{1}{2}} - (S_k)_{n+\frac{1}{2}}^{j-\frac{1}{2}}\Big),\end{aligned} \tag{26}$$

where

$$(S_k)_n^j = \frac{\Delta x}{2}(V_{kx})_n^j + \frac{\Delta t}{\Delta x}(F_k)_n^j + \frac{(\Delta t)^2}{4\Delta x}(F_{kt})_n^j. \tag{27}$$

For conservative flow variables slopes, the numerical oscillations can be reduced through limiting formulations near a discontinuity.

$$(V_k')_{n\pm\frac{1}{2}}^j = (V_k)_{n\pm\frac{1}{2}}^{j-\frac{1}{2}} + \frac{\Delta t}{2}(V_{kt})_{n\pm\frac{1}{2}}^{j-\frac{1}{2}}, \quad k = 1, 2. \tag{28}$$

Tractable constant $\gamma \geqslant 0$ mostly have value $\gamma = 1$or $\gamma = 2$ and

$$V(x_-, x_+;\gamma) = \frac{|x_+|^\gamma x_- + |x_-^\gamma| x_+}{|x_+^\gamma| + |x_-^\gamma|}. \tag{29}$$

Moreover,

$$(V_{kx_+})_n^j = \frac{(V_k')_{n+\frac{1}{2}}^j - (V_k)_n^j}{\Delta x/2}, \quad (V_{kx_-})_n^j = \frac{(V_k)_n^j - (V_k')_{n-\frac{1}{2}}^j}{\Delta x/2}, \quad . \tag{30}$$

and

$$(V_k')_{n\pm\frac{1}{2}}^j = (V_k)_{n\pm\frac{1}{2}}^{j-\frac{1}{2}} + \frac{\Delta t}{2}(V_{kt})_{n\pm\frac{1}{2}}^{j-\frac{1}{2}}, \quad k = 1, 2. \tag{31}$$

2.2 Central scheme in one dimensional space

The high-resolution central scheme [46] is discussed briefly. This scheme has two parts, One is the Predictor and the second part is Corrector. This is known as a Predictor-Corrector method. The first part of the Predictor relates the prediction of the midpoint values of the cell. The second corrector part relates to the average values of the cell. By mathematically, the Predictor formula for central scheme is

$$(V)_i^{m+\frac{1}{2}} = (V)_i^m + \frac{\beta}{2}(F)^x(V)^m, \tag{32}$$

Moreover, updated values at the next time step is obtained through corrector step, as defined below

$$\begin{aligned}(V)_{i+\frac{1}{2}}^{m+\frac{1}{2}} = \frac{1}{2}\Big((V)_i^m + (V)_{i+1}^m\Big) + \frac{1}{8}\Big((V)_i^x - (V)_{i+1}^x\Big) \\ - \beta\Big((F)_{i+1}^{m+\frac{1}{2}} - (F)_i^{m+\frac{1}{2}}\Big) - \beta\Big((S)_{i+1}^{m+\frac{1}{2}} - (S)_i^{m+\frac{1}{2}}\Big),\end{aligned} \tag{33}$$

here β=$\frac{\Delta t}{\Delta x}$. Moreover, $\frac{1}{\Delta x}F^x(V^i)$ is approximated derivative of $F(V(t, x))$

$$\frac{1}{\Delta x}F^x(V^i) = \frac{\partial}{\partial x}F(V(t,x)) + O(\Delta x), \tag{34}$$

The fluxes $F^x(V^i)$ calculated through similar process as described for v^x in Eq. (35)

$$V_i^x = MM\Big(\theta\Delta V_{i+1/2}, \frac{\theta}{2}(\Delta V_{i+1/2} + \Delta V_{i-1/2}), \theta\Delta V_{i-1/2}\Big), \tag{35}$$

here θ is the parameter $\theta \in [1, 2]$ and the central differencing is denoted by Δ, which is defined as

$$\Delta V_{i+1/2} = V_{i+1} - V_i, \tag{36}$$

where MM = The min-mod nonlinear limiter.

3 Numerical simulation

In this section, we will discuss the different numerical test problems for one-dimensional repulsive chemotaxis models, with the help of our proposed numerical scheme i-e CE/SE method, and thereafter, results are also compared with NT central scheme.

3.1 Test problems for parabolic model in one space dimension

Problem 1 Let us consider one-dimensional repulsive chemotaxis model system with periodic initial conditions are defined as.

$$p(x) = 3\left(\frac{x^2}{2} - \frac{x^3}{3}\right), \quad x \in [0, 1], \tag{37}$$

whereas, the concentration $q(x)$ is

$$q(x) = x(1 - x), \quad x \in [0, 1]. \tag{38}$$

The comparison of numerical results of density and concentration on 200-grids for different values of time and epsilon are shown in Figs. 2 and 3. It is observed that

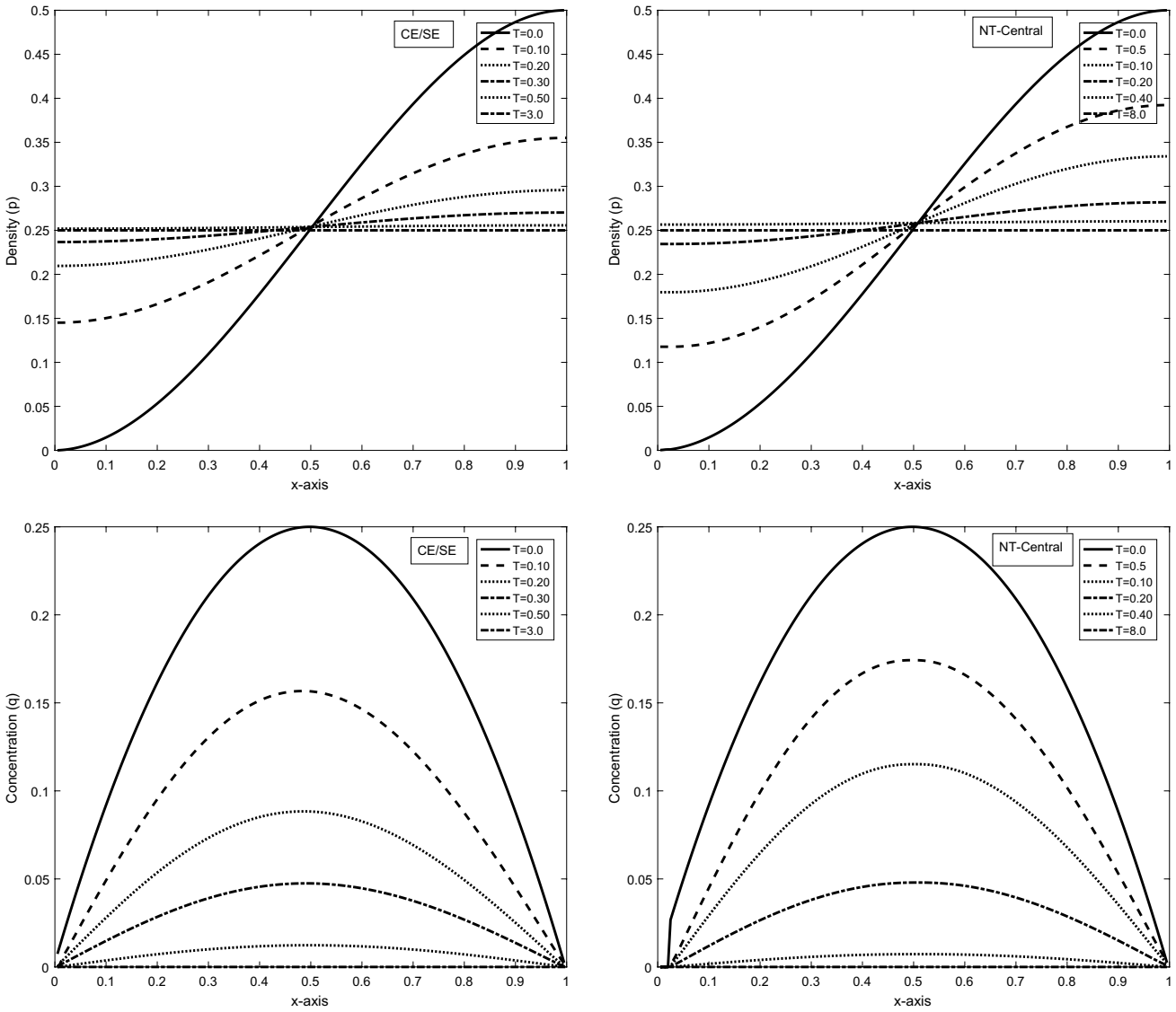

Fig. 2 Numerical results of CE/SE and NT central schemes for different values of time on 200 grid points of test problem 1

solution profiles for CE/SE scheme converges to 0.25 and 0 rapidly for different values of epsilon as compared to the NT-central scheme. Similar analysis and results were also reported in [61]. So the CE/SE scheme shows good results as compared to NT-central scheme (Figs. 4, 5).

Problem 2 Consider smooth initial data for one-dimensional chemotaxis system.

$$p(0,x) = 1 + 0.2\cos(\pi x), \quad x \in [-1,1], \tag{39}$$

here, chemo-attractant $c(x)$ is defined as

$$q(x) = \exp(-16x * x), \quad x \in [-1,1]. \tag{40}$$

Here '*' is the usual multiplication. This smooth initial data of the test problem was also considered and analyzed in [43]. The numerical errors L^∞ and L^1 along-with convergence rate for L^1 error are enlisted in Table 1. From Table 1 the presented numerical scheme is almost second-order accurate on 200-grids and 400-grids. Whereas, for 800-grids the jumps and peaks reduced the order of accuracy.

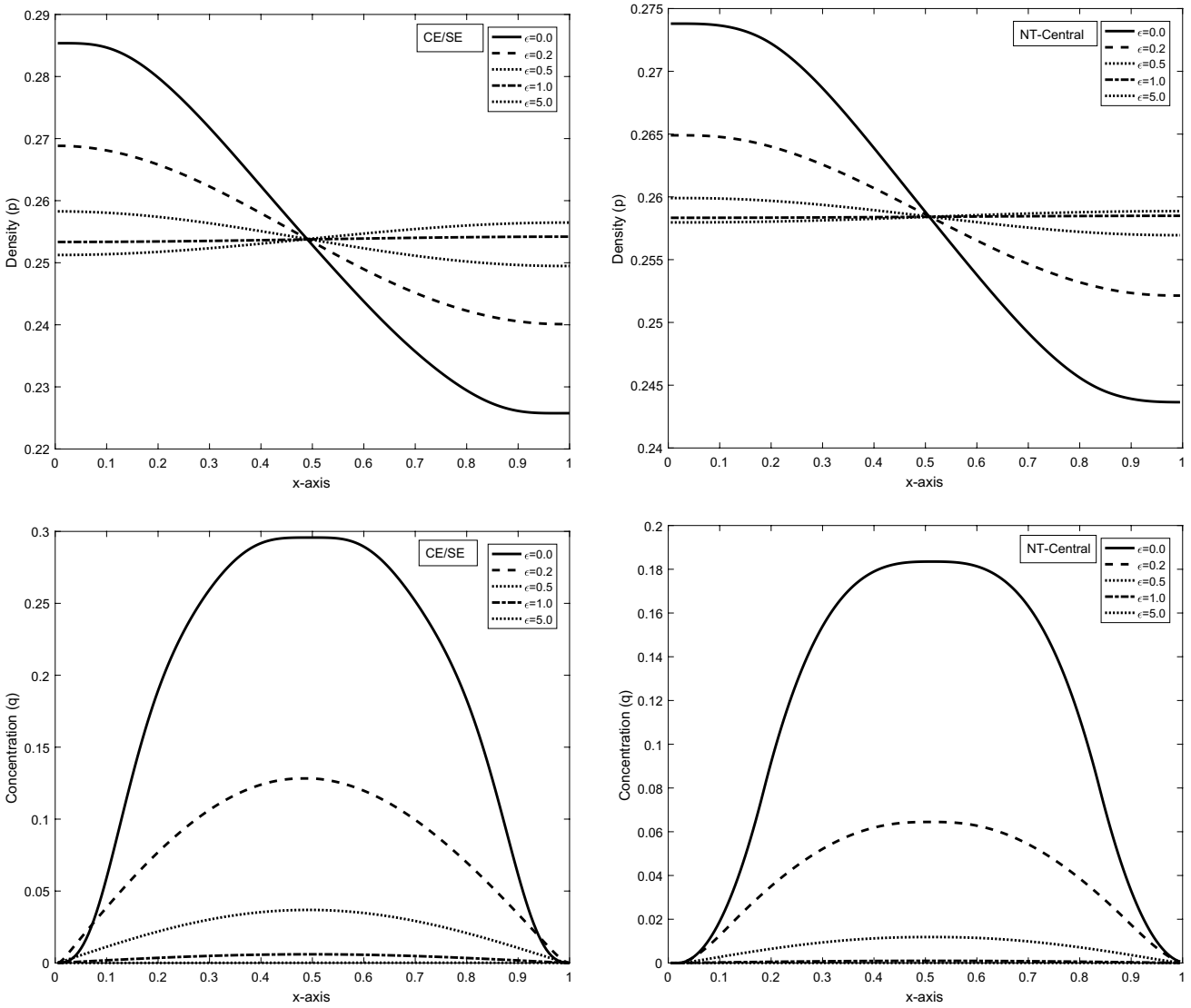

Fig. 3 Numerical results of CE/SE and NT central schemes for different values of epsilon on 200 grid points of test problem 1

Errors are computed with the help of reference solution and computed solution profile of both schemes (CE/SE and Nessyahu Tadmor central) are displayed in the Table 2 with different (100, 200, 400, 800) grids points. Furthermore, Table 2 displayed CPU time in seconds. We obtained the reference solution at 1600-grid points. The second-order solution, efficiency, and robustness of the proposed scheme is validated through the results of computation time and error analysis. Certainly, identical behavior was also perceived in [43] with other numerical methods. It can be seen that with the increase in the number of grid points, errors decrease rapidly in CE/SE scheme. Error plots are given in Figs. 6 and 7. The numerical results of density and concentration on 200-grids are shown in Fig. 4. Since the initial density and concentration depend on continuous functions, so from Fig. 4 smooth transitions are examined in all quantities. The CE/SE scheme shows good computational outcome when correlated to the NT-central algorithm. As well, our suggested numerical scheme captured and resolved all peaks more accurately and efficiently. Similar analysis and results were also given in [43] and reference therein.

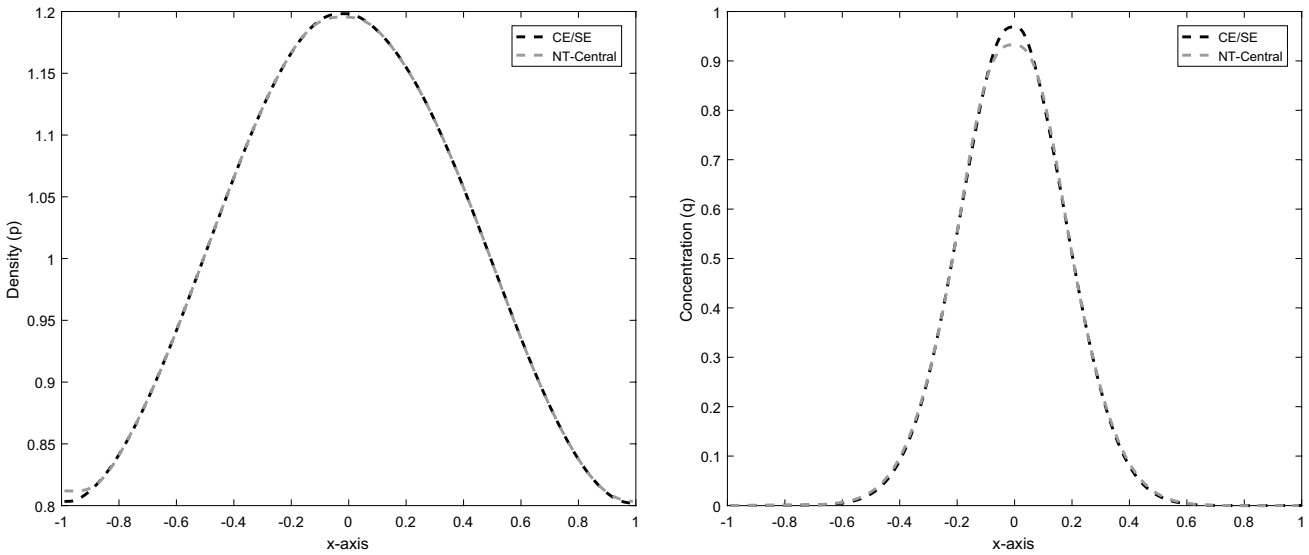

Fig. 4 Comparison of numerical results of CE/SE and NT central schemes on 200 grid points of test problem 2

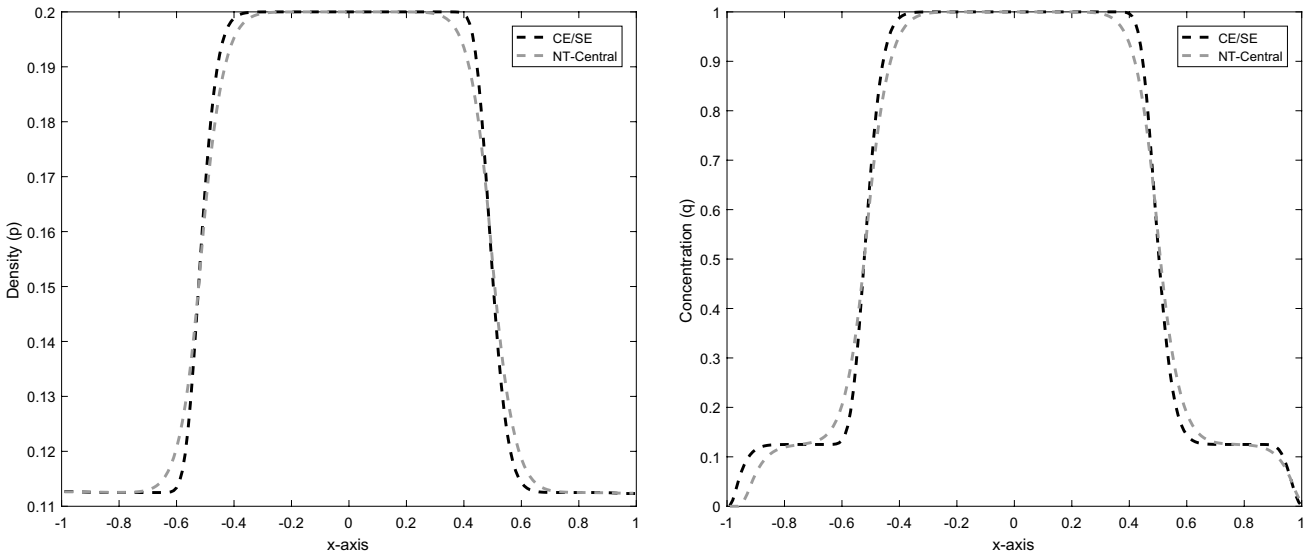

Fig. 5 Comparison of numerical results of CE/SE and NT central schemes on 200 grid points of test problem 3

Table 1 Numerical errors for different number of grid points

Grid numbers	Density (p)			Concentration (q)		
	L^∞	L^1	Rate	L^∞	L^1	Rate
100	0.0239	0.0304	–	0.0400	0.1828	–
200	0.0120	0.0071	2.10	0.0200	0.0347	2.39
400	0.0060	0.0019	1.90	0.0100	0.0061	2.51
800	0.0030	0.00051	1.86	0.0050	0.0015	1.95

Table 2 Comparison of numerical errors at different grid points

Method	100-Grid-points		
	Density (p)	Concentration (q)	CPU-time (sec)
CESE	0.0304	0.1828	10.76
NT central	0.2317	0.3643	29.47
	200-Grid-points		
CESE	0.0071	0.0347	19.52
NT central	0.0582	0.2613	40.59
	400-Grid-points		
CESE	0.0019	0.0061	33.8
NT central	0.0136	0.0762	84
	800-Grid-points		
CESE	0.00051	0.0015	61.11
NT central	0.0018	0.0135	136.7

Problem 3 To examine the steady-state conservation, time-independent solution is considered as

$$p(0,x) = \frac{1 + c(x)}{10}, \tag{41}$$

$$q(x) = \begin{cases} 1, & if \ \ |\, x \,| \leq \frac{1}{2}, \\ 0.125, & \text{elsewhere.} \end{cases} \tag{42}$$

This smooth initial data of the test problem was also considered and analyzed in [43]. The numerical results of density and concentration on 200-grids are shown in Fig. 5. The density is considered small in the regions $x \in [-1.0, -0.5]$ and $x \in [0.5, 1.0]$. It can be noticed from the Fig. 5, that around $x = -0.5$ the density rapidly

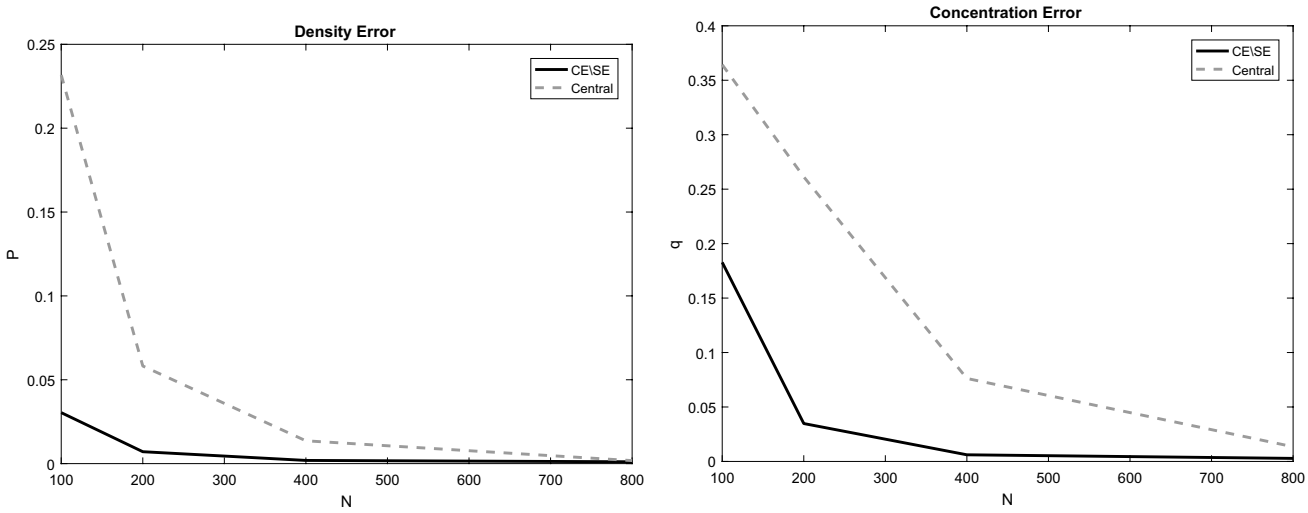

Fig. 6 L^1-error plots of CE/SE and NT central schemes on different grid points

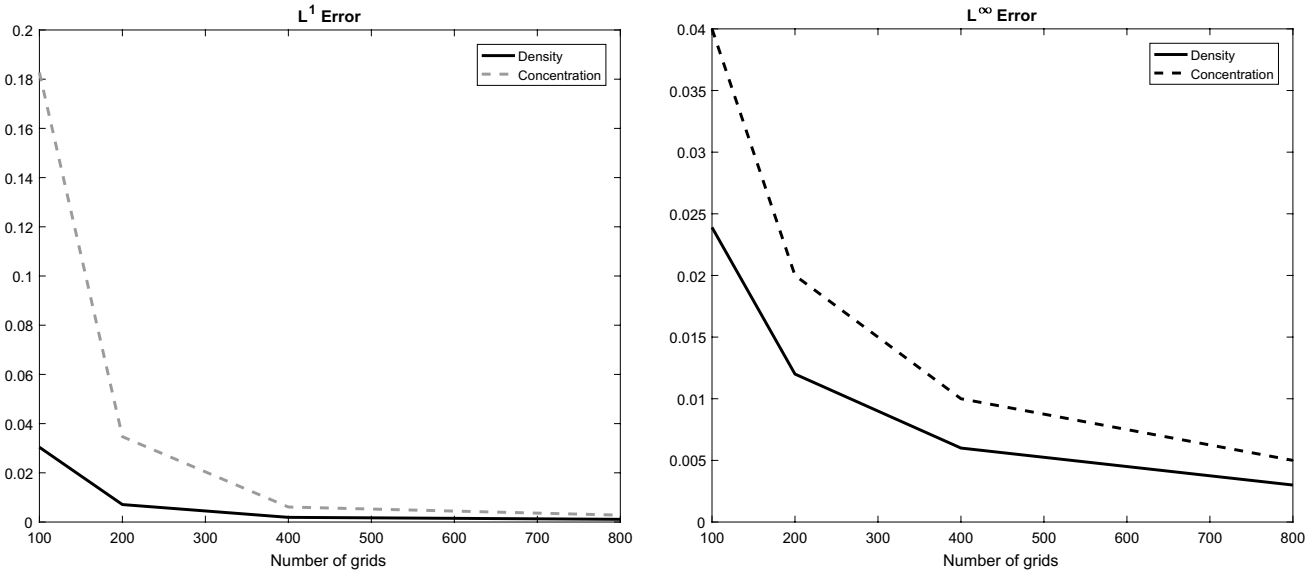

Fig. 7 Numerical errors in the results of CE/SE scheme

increases and continued till $x = 0.5$. The same behavior can also be observed in the concentration profile. The CE/SE scheme shows good results as compared to NT-central scheme. Moreover, our suggested numerical scheme captured and resolved all discontinuities more accurately and efficiently. Similar analysis and results were also described in [43] and references therein.

4 Conclusions

A more capable and accurate numerical procedure is proposed for a highly nonlinear time-dependent system of partial differential equations for repulsive chemotaxis which is based on splitting scheme strategy. This scheme was introduced by Chang [59] and his team. The method is extended for the solution in one space dimension. This scheme is based on combined treatment of both space and time. Moreover, it uses the derivatives of conserved variables to reduce numerical diffusion. Furthermore, the central scheme introduced by Nessyahu and Tadmor was also implemented for validation and comparison. Several benchmark test problems are simulated in one-dimensional space. It was evident that the computational outcome of both, the proposed method and Nessyahu and Tadmore (NT) central scheme were agreeing well with the results presented in already published literature. Moreover, both schemes can capture the steep and sharp changes in the solution profile more accurately and efficiently. However, the proposed method has performed splendidly well for such solutions (sharp and steep discontinuities, narrow peaks). It is also observed that solution profiles p and q converge to 0.25 and 0 faster through CE/SE as analyzed with central schemes by Nessyahu and Tadmor. The presented method CE/SE produced less numerical errors in results and more efficient in contrast with NT central scheme on staggered grids.

Author Contributions All authors contributed equally to the writing of this paper. All authors read and approved the nal manuscript.

Compliance with Ethical Standards

Conflict of interest All authors declare that they have no competing interests.

Ethical approval This article does not contain any studies with human participants or animals performed by any of the authors.

References

1. Goldstein RE (1996) Traveling-wave chemotaxis. Phys Rev Lett 77(4):775
2. Lee KJ, Cox EC, Goldstein RE (1996) Competing patterns of signaling activity in dictyostelium discoideum. Phys Rev Lett 76(7):1174
3. Brenner MP, Levitov LS, Budrene EO (1998) Physical mechanisms for chemotactic pattern formation by bacteria. Biophys J 74(4):1677–1693
4. Budrene EO, Berg HC (1991) Complex patterns formed by motile cells of *Escherichia coli*. Nature 349(6310):630–633
5. Budrene EO, Berg HC (1995) Dynamics of formation of symmetrical patterns by chemotactic bacteria. Nature 376(6535):49–53
6. Welch R, Kaiser D (2001) Cell behavior in traveling wave patterns of myxobacteria. Proc Nat Acad Sci 98(26):14907–14912
7. Murray JD (2002) Mathematical biology. An introduction, interdisciplinary applied mathematics, 17 Springer Verlag, New York. In: Mathematical Biology. II spatial models and biomedical applications. Third edition. Interdisciplinary applied mathematics, 18
8. Adler J (1966) Chemotaxis in bacteria. Science 153(3737):708–716
9. Keller EF, Segel LA (1970) Initiation of slime mold aggregation viewed as an instability. J Theor Biol 26(3):399–415
10. Keller EF, Segel LA (1971) Model for chemotaxis. J Theor Biol 30(2):225–234
11. Keller EF, Segel LA (1971) Traveling bands of chemotactic bacteria: a theoretical analysis. J Theor Biol 30(2):235–248
12. Childress S (1984) Chemotactic collapse in two dimensions. In: Modelling of patterns in space and time, Springer, Berlin, Heidelberg, pp 61–66
13. Horstmann D (2003) From 1970 until present: the Keller–Segel model in chemotaxis and its consequences
14. Alt W, Lauffenburger DA (1987) Transient behavior of a chemotaxis system modelling certain types of tissue inflammation. J Math Biol 24(6):691–722
15. Lin CS, Ni WM, Takagi I (1988) Large amplitude stationary solutions to a chemotaxis system. J Differ Equ 72(1):1–27
16. Winkler M (2011) Global solutions in a fully parabolic chemotaxis system with singular sensitivity. Math Methods Appl Sci 34(2):176–190
17. Segel LA (1977) A theoretical study of receptor mechanisms in bacterial chemotaxis. SIAM J Appl Math 32(3):653–665
18. Sherratt JA, Sage EH, Murray JD (1993) Chemical control of eukaryotic cell movement: a new model. J Theor Biol 162(1):23–40
19. Luca M, Chavez-Ross A, Edelstein-Keshet L, Mogilner A (2003) Chemotactic signaling, microglia, and Alzheimer's disease senile plaques: is there a connection? Bull Math Biol 65(4):693–730
20. Sleeman BD, Levine HA (1997) A system of reaction-diffusion equations arising in the theory of reinforced random walks. SIAM J Appl Math 57(3):683–730
21. Stevens A, Othmer HG (1997) Aggregation, blowup, and collapse: the ABC's of taxis in reinforced random walks. SIAM J Appl Math 57(4):1044–1081
22. Yang Y, Chen H, Liu W (2001) On existence of global solutions and blow-up to a system of reaction-diffusion equations modelling chemotaxis. SIAM J Math Anal 33(4):763–785
23. Wang Z, Hillen T (2008) Shock formation in a chemotaxis model. Math Methods Appl Sci 31(1):45–70
24. Li T, Wang ZA (2009) Nonlinear stability of traveling waves to a hyperbolic-parabolic system modelling chemotaxis. SIAM J Appl Math 70(5):1522–1541

25. Li T, Wang ZA (2010) Nonlinear stability of large amplitude viscous shock waves of a generalized hyperbolic-parabolic system arising in chemotaxis. Math Models Methods Appl Sci 20(11):1967–1998
26. Li T, Wang ZA (2011) Asymptotic nonlinear stability of traveling waves to conservation laws arising from chemotaxis. J Differ Equ 250(3):1310–1333
27. Zhang M, Zhu C (2007) Global existence of solutions to a hyperbolic-parabolic system. Proc Am Math Soc 135(4):1017–1027
28. Jun G, Jixiong X, Huijiang Z, Changjiang Z (2009) Global solutions to a hyperbolic-parabolic coupled system with large initial data. Acta Mathematica Scientia 29(3):629–641
29. Li D, Li T, Zhao K (2011) On a hyperbolic-parabolic system modelling chemotaxis. Math Models Methods Appl Sci 21(08):1631–1650
30. Li T, Pan RH, Zhao K (2012) Global dynamics of a chemotaxis model on bounded domains with large data. SIAM J Appl Math 72(1):417–443
31. Li T, Pan R, Zhao K (2012) Global dynamics of a hyperbolic-parabolic model arising from chemotaxis. SIAM J Appl Math 72(1):417–443
32. Li T, Wang ZA (2012) Steadily propagating waves of a chemotaxis model. Math Biosci 240(2):161–168
33. Emako C, Gayrard C, Buguin A, De Almeida LN, Vauchelet N (2016) Traveling pulses for a two-species chemotaxis model. PLoS Comput Biol 12(4):e1004843
34. Kurganov A, Lukacova-Medvidova M (2014) Numerical study of two-species chemotaxis models. Discrete Contin Dyn Syst Ser B 19(1):131–152
35. Chertock A, Epshteyn Y, Hu H, Kurganov A (2018) High-order positivity-preserving hybrid finite-volume-finite-difference methods for chemotaxis systems. Adv Comput Math 44(1):327–350
36. Wang ZA (2013) Mathematics of traveling waves in chemotaxis–review paper–. Discrete Conti Dyn Syst B 18(3):601–641
37. Tao Y, Wang L, Wang ZA (2013) Large time behavio of a parabolic-parabolic chemotaxis model with logarithmic sensitivity in one dimension. Discrete Contin Dyn Syst Ser B 18(3):821–845
38. Li H, Zhao K (2015) Initial boundary value problems for a system of hyperbolic balance laws arising from chemotaxis. J Differ Equ 258(2):302–338
39. Martinez V, Wang Z, Zhao K (2018) Asymptotic and viscous stability of large-amplitude solutions of a hyperbolic system arising from biology. Indiana Univ Math J 67(4):1383–1424
40. Hou Q, Wang ZA, Zhao K (2016) Boundary layer problem on a hyperbolic system arising from chemotaxis. J Differ Equ 261(9):5035–5070
41. Li J, Li T, Wang ZA (2014) Stability of traveling waves of the Keller–Segel system with logarithmic sensitivity. Math Models Methods Appl Sci 24(14):2819–2849
42. Hillen T (2002) Hyperbolic models for chemosensitive movement. Math Models Methods Appl Sci 12(07):1007–1034
43. Filbet F, Shu CW (2005) Approximation of hyperbolic models for chemosensitive movement. SIAM J Sci Comput 27(3):850–872
44. Chang SC (1995) The method of space-time conservation element and solution element—a new approach for solving the Navier–Stokes and Euler equations. J Comput Phys 119(2):295–324
45. Chang SC, Wang XY, Chow CY (1999) The space-time conservation element and solution element method: a new high-resolution and genuinely multidimensional paradigm for solving conservation laws. J Comput Phys 156(1):89–136
46. Qamar Shamsul, Ashraf Waqas (2013) Application of central schemes for solving radiation hydrodynamical models. Comput Phys Commun 184(5):1349–1363
47. Qamar S, Ashraf W (2014) A space-time CE/SE method for solving hyperbolic heat conduction model. Int J Comput Methods 11(01):1350048
48. Liu M, Wang JB, Wu KQ (2007) The direct aero-acoustics simulation of flow around a square cylinder using the CE/SE scheme. J Algorithms Comput Technol 1(4):525–538
49. Qamar S, Zia S, Ashraf W (2014) The space-time CE/SE method for solving single and two-phase shallow flow models. Comput Fluids 96:136–151
50. Qamar S, Mudasser S (2010) On the application of a variant CE/SE method for solving two-dimensional ideal MHD equations. Appl Numer Math 60(6):587–606
51. Wang XY, Chen CL, Liu Y (2002 June) The space-time CE/SE method for solving Maxwell's equations in time-domain. In: IEEE Antennas and propagation society international symposium (IEEE Cat. No. 02CH37313). IEEE, vol 1, pp 164–167
52. Nessyahu H, Tadmor E (1990) Non-oscillatory central differencing for hyperbolic conservation laws. J Comput Phys 87(2):408–463
53. LeVeque RJ, Leveque RJ (1992) Numerical methods for conservation laws, vol 132. Birkhäuser, Basel
54. Huynh HT (1995) Accurate upwind methods for the Euler equations. SIAM J Numer Anal 32(5):1565–1619
55. Zhao G, Yu X (2015) The high order control volume discontinuous Petrov–Galerkin finite element method for the hyperbolic conservation laws based on Lax–Wendroff time discretization. Appl Math Comput 252:175–188
56. Shu CW, Osher S (1988) Efficient implementation of essentially non-oscillatory shock-capturing schemes. J Comput Phys 77(2):439–471
57. Zhu J, Qiu J (2009) Hermite WENO schemes and their application as limiters for Runge–Kutta discontinuous Galerkin method, III: unstructured meshes. J Sci Comput 39(2):293–321
58. Qamar S, Yousaf M (2012) The space-time CESE method for solving special relativistic hydrodynamic equations. J Comput Phys 231(10):3928–3945
59. Zhang ZC, Yu SJ, Chang SC (2002) A space-time conservation element and solution element method for solving the two-and three-dimensional unsteady Euler equations using quadrilateral and hexahedral meshes. J Comput Phys 175(1):168–199
60. Chang SC (2010) A new approach for constructing highly stable high order CESE schemes. In: 48th AIAA Aerospace sciences meeting including the new horizons forum and aerospace exposition (p 543)
61. Wang ZA, Zhao K (2013) Global dynamics and diffusion limit of a one-dimensional repulsive chemotaxis model. Commun Pure Appl Anal 12:3027–3046